# Design study of a high-resolution breast-dedicated PET system built from cadmium zinc telluride detectors

Hao Peng, *Member, IEEE*, P. D. Olcott , G. Pratx, A. M. K. Foudray, G. Chinn, C. S. Levin , *Member, IEEE*

***Abstract*– We are developing a dual-panel cadmium zinc telluride (CZT) detector positron emission tomography (PET) system dedicated to breast imaging. The proposed system consists of two 4 cm thick 12x15 cm$^2$ area CZT panels with adjustable separation, which can be put in close-proximity to breasts and/or axillary nodes and results in high photon sensitivity. In this project, the performance of the proposed CZT dual panel PET system was investigated using Monte-Carlo simulation. Expected system performance is predicted due to CZT's superior energy resolution, the high photon sensitivity, and the uniform spatial resolution throughout field-of-view (FOV). The dependency of system reconstructed resolution on depth-of-interaction (DOI) resolution was also studied.**

## I. Introduction

Positron emission tomography (PET) has shown promise for more specific identification of cancer due to its unique ability to sense and visualize increased bio-chemical and molecular changes in malignant compared to healthy tissue [1]-[3]. However, PET has not been incorporated into standard practice for breast cancer patient evaluation mainly due to following factors [4]: awkward, low coincidence photon detection efficiency geometry for breast imaging; non-optimal spatial and energy resolutions for early breast cancer identification; relatively long scan times; and the lack of tracers with adequate specificity. Aiming to address the first three issues, we are developing a compact, high performance breast-dedicated PET system deploying novel CZT detectors.

The proposed system is shown in Fig .1. The system is designed as two panels, which can be put in close-proximity to breasts and/or axillary nodes. We believe that such dual-panel geometry would result in high photon sensitivity, while minimizing background effects from potential uptake of tracer in the nearby heart. In addition, the open gap between two panels can also facilitate the breast biopsy procedure. In addition, compared to conventional scintillator based PET detectors, CZT detectors exhibit much better energy resolution for 511 keV photons (<3% full-width-half-maximum (FWHM)) due to improved energy-to-signal conversion though the time resolution is relatively poor (~ 8 ns FWHM) [5]. Moreover, the cross-strip readout scheme for CZT detector implements the pixellation electronically instead of cutting scintillator into small pixels, as shown in Fig. 1c. This enables the system to maintain high intrinsic spatial resolution and also reduce the required readout channels compared against a square pixelled anode readout scheme. Furthermore, in our proposed system, the 511 keV photon will enter the detector in an edge-on manner, providing 4 cm thickness of detector along the photon's path to increase the detection efficiency. The photon interaction depth information can be realized by the cathode readout strips. Such three dimensional spatial resolution will facilitate uniform spatial resolution throughout the full field-of-view (FOV).

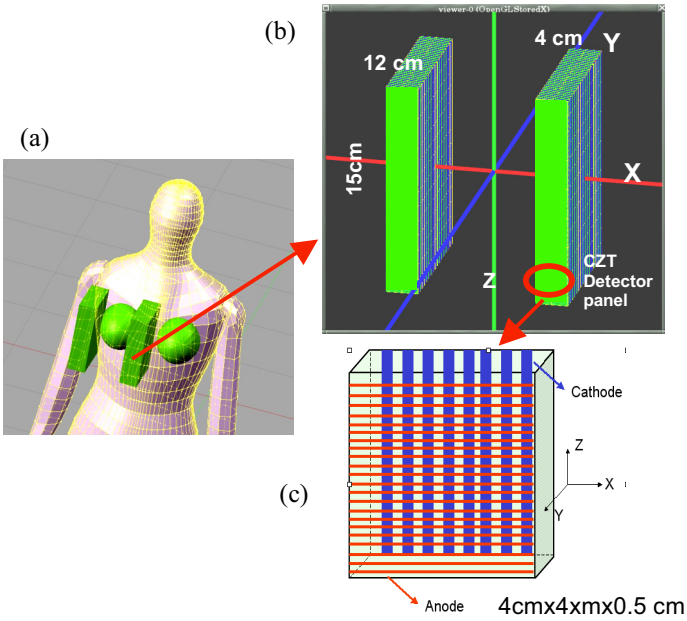


Fig. 1: (a) Illustration of the proposed dual panel CZT-based PET system for breast cancer imaging. (b) Diagram of dual panel breast-dedicated PET system consisting of 180 cross-strip CZT detector modules each of size 4 x 4x 0. 5 cm$^3$ with 25 µm inter-module spacing, giving a packing ratio of over 99%. (c) Each panel has dimensions 4x12x15 cm$^3$ and the separation between the panels in this study is 4 cm.

## II. Material and Methods

### A. Simulation tool and system description

GATE (Geant4 Application in Tomographic Emission) was used to study photon sensitivity and count rate performance [6]. GRAY, a new photon transport simulation package we have developed and validated against GATE, was used for the system resolution and contrast study due to its significantly reduced simulation time.

Manuscript received November 18, 2007. This work was supported in part by grants R01CA120474 from NIH and 12IB-0092 from California Breast Cancer Research Program.

Hao Peng is with the Department of Radiology and Molecular Imaging Program, Stanford University, Stanford, CA. (telephone: 650-736-7093, e-mail: haopeng@stanford.edu).

P. D. Olcott, G. Pratx, A. M. K. Foudray, G. Chinn, C. S. Levin are with the Department of Radiology and Molecular Imaging Program, Stanford University, Stanford, CA. (telephone: 650-736-7211, e-mail: cslevin@stanford.edu).

### B. Point source coincidence photon sensitivity

A point source with 100 μCi was translated from the center of FOV to the edge of the X, Y, and Z directions. The coordinate location was indicated in Fig. 1. The detector energy resolution was 3% FWHM at 511 keV and the coincidence time resolution was 8 ns FWHM [5], which were used for all simulation studies. The energy window and time window settings were chosen to be twice those resolution values. The number of coincidence 511 keV photons was approximately 1 million.

### C. Coincidence count rate studies

To investigate the performance of our proposed CZT based PET system with superior energy resolution and relatively poor time resolution, the noise equivalent count (NEC) rate was studied. A simplified model was introduced to mimic the geometry for PET breast imaging, as shown in Fig. 2. The hot heart and warm torso compartment were put adjacent to the breast tissue compartments. The breast compartment completely filled the volume between two CZT panels. The sizes for all compartments in our simulation are provided in Fig. 2, though the accuracy of the model might be further improved and the possibility of introducing lead shielding at the edge of two panels is under study.

The activity concentration in breast phantom is 0.1 μCi/cm3 and the total activity inside breast phantom is 200 μCi, which are chosen from published studies for clinical breast cancer imaging [4]. The NEC is calculated as:

$$NEC = \frac{T^2}{T + S + 2R} \qquad (1)$$

where T, S and R are rates of true, scatter, and random coincidence events. Since T, S and R all depend on the preset energy window and time window, the dependency of NEC on various ranges of energy window and time window were studied. The optimum operating window settings were necessary to complete other studies in this work. For each set of simulations, the number of coincidence 511 keV photons was approximately 6 million.

### D. System spatial resolution study

To investigate system spatial resolution, a plane (at X=0, refer to Fig.1) consisting of spherical sources of various diameters was imaged. No hot background was considered in the resolution study. The spherical source diameters were 2.5 mm, 3.0 mm, 3.5 mm and 4.0 mm and they were located in four quadrants of the plane, respectively, as shown in the Results section. For each quadrant, the distance between the centers of two tumor sources is twice the diameter of sources.

For the cross strip readout scheme, the space between anode strips determines the Z direction resolution. The space between cathode strips determined system DOI resolution along X direction. The position along Y direction can be extracted from the ratio between signals from anodes and cathodes. In this study, the system resolution along Y and Z direction were assumed to be 1 mm based on previous studies [5] while the resolution along X direction was varied to study DOI effect on reconstructed system resolution. The coordinates obtained from simulation events were rebinned to the center of the nearest 3D detector voxel element. A list-mode 3D Ordered-Subset Expectation Maximization (OSEM) image reconstruction algorithm was used and the FWHM for reconstructed sphere sources as a function of depth-of-interaction (DOI) resolution was studied.

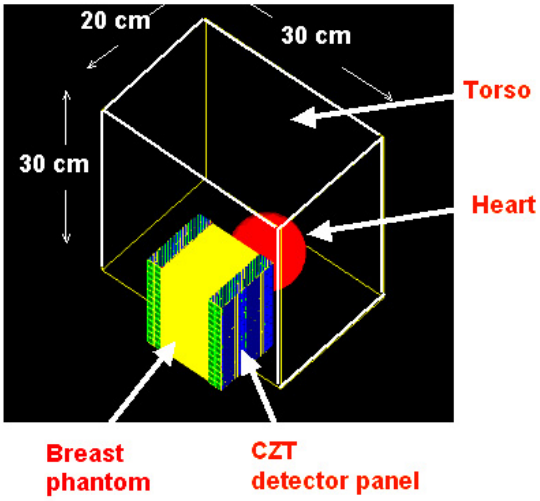


Fig. 2: The simulated model for system NEC studies. A hot spherical heart with 10 cm diameter and a warm torso of dimensions of 30x20x30 $cm^3$ are adjacent to breast phantom. Activity concentration ratio assumed for breast-heart-torso was 1:10:1 and the detectors were unshielded.

## III. Results

### A. Coincidence photon sensitivity

The photon sensitivity as a function of distance from the center is shown in Fig. 3 for a point source. At the center of FOV, the system sensitivity is about 32.5%, which is much higher than that of conventional whole body PET systems [4]. Though the sensitivity decreases as the point source moves away from the center, the system is able to achieve a high sensitivity better than 15% within 4 cm of the center of the FOV for all three directions. Such increased sensitivity is attributed the dual panel locating in close proximity to the breast as well as the high packing ratio of 4 cm thick detector modules. Such advantages will help to improve system signal-to-noise ratio and lesion contrast recovery, or alternatively reduce the image time.

### B. Coincidence count rate studies

Fig.4 shows the system NEC as a function of both coincidence time window and energy windows.

The NEC reaches a peak value (~42000 cts/sec) around 8-10 ns time window and 459-463 keV energy window, as shown in Fig. 4a. The decrease following the peak for all energy windows is attributed to the higher random events due to the heart and torso background. Moreover, it is noticed that for those narrower energy windows (507-515 keV and 503-519 keV), NEC peaks at a larger time window (~14 ns) compared to that of wider energy windows due to the fact that a portion of random events are rejected by applying a narrow energy window. As shown in Fig. 4b, the NEC reaches a plateau of the same amplitude as shown in Fig. 4a, at around

10% energy windows for all time windows. Further increasing energy window will have no effect on NEC performance.

The high NEC is attributed to the good energy resolution, which can improve the rejection of both scatter coincidences as well as single photons that have scattered, thus also rejecting random coincidences.

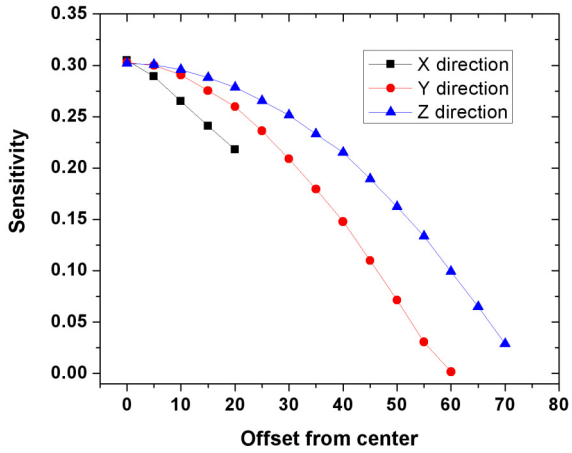


Fig. 3: System sensitivity with a point source of 100μCi at the system center as a function of distance (mm) from the center along X, Y, Z directions. The energy window is 10% and the time window is 10 ns.

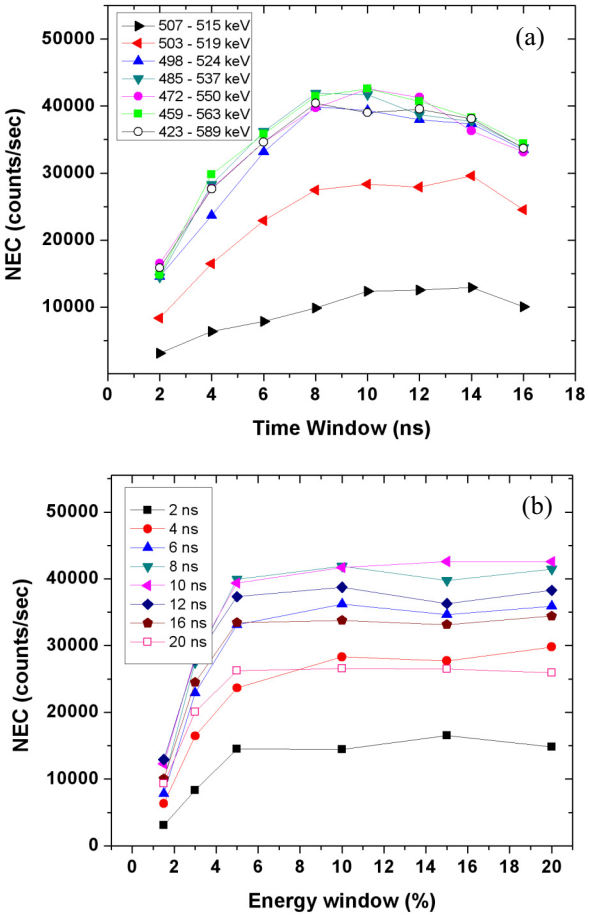


Fig. 4: System NEC as a function of different time window and energy window centered at 511 keV for 4 cm panel separation. The peak NEC reaches a plateau at ~42,000 counts/sec around 8-10 ns time window (a) and 10% energy window at 511 keV (b).

*C. Reconstructed spatial resolution study*

Fig.5 shows the reconstructed image of spherical sources (no background) of three different DOI resolutions (2 mm, 5 mm and 10 mm) respectively, using list mode 3D-OSEM algorithm (subset: 1, iteration: 3). No normalization and attenuation correction was made for the image reconstruction.

The proposed system's resolution, both in-plane (Fig. 5a) and cross-plane (Fig. 5b) is dependent on DOI resolution. The in-plane resolution is defined as the reconstructed sphere FWHM in YZ plane (along Y or Z direction). The cross-plane resolution is defined as the reconstructed sphere FWHM in XZ plane (along X direction). As shown in Fig. 5, for both cases, the spheres are better resolved as DOI improves and this is more significant for the cross-plane resolution. The resolution improvement is likely due to the decreased spacing and the increased density of line-of-responses (LORs), as DOI resolution improves.

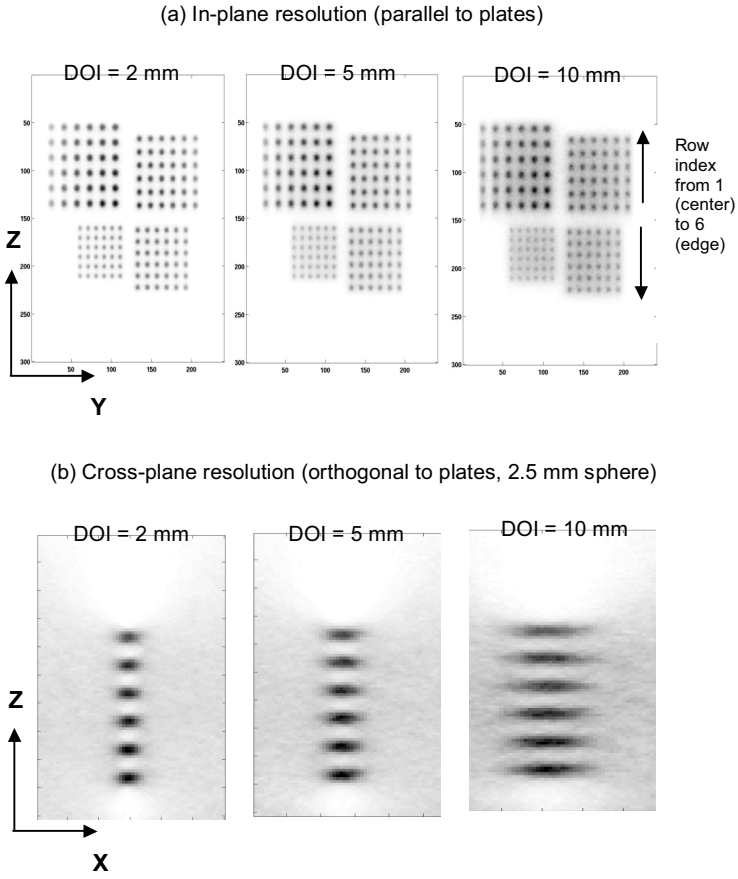


Fig. 5: Reconstructed planes through spherical sources for different depth-of-interaction (DOI) resolution (2 mm, 5 mm and 10 mm), X=0. The simulated tumor diameters are 2.5 mm, 3.0 mm, 3.5 mm and 4.0 mm placed on a plane midway between the two panels separated by 4 cm. (a) The reconstructed sphere in-plane FWHM and (b) cross-plane (XY).

The quantitative analysis is provided in Fig. 6. The 6x6 sphere array in each quadrant was analyzed to study the resolution uniformity throughout the FOV. The average and uncertainties of FWHMs of six Gaussian functions were referred to as "reconstructed sphere FWHM" as shown in Fig 6. The goodness of all fits varies from 0.90 to 1.10. The

significant error bars are attributed to the resolution degradation from the center of the plane towards the edge of the plane. It should be noted that the spheres smaller than 2.5 mm were not chosen since it would be difficult to achieve good fitting results since we used 0.5 mm pixel size in the image reconstruction.

As shown in Fig. 6a and 6b, the dependence of in-plane and cross-plane resolution on the DOI resolution was achieved, for the central plane (X=0). The results provide the general guidance regarding how to design cathode strip spacing for a given resolution requirements in systems deploying a dual panel geometry. For smaller tumor sizes (<3.0 mm diameter), DOI resolution (pitch of cathode cross strips) should be better than 5 mm.

The uniformity of the spatial resolution of the proposed CZT system across the FOV is shown in Fig. 6c and 6d. The row index corresponds to the different positions of six rows within a single YZ plane and ranges from 1 to 6, as illustrated in Fig. 5a. For both X=0 and X=1.5 cm, the reconstructed in-plane and cross-plane resolution show no dependency on the row index, which means that the system is able to achieve uniform resolution from the center towards the edge of the FOV for a single YZ plane. However, the dependence of in-plane resolution on the plane's position (X value) is observed in Fig. 6c and this is most noticeable for 2.5 mm spheres. Cross-plane resolution shows no such dependency on the row index (Fig. 6d). More detailed studies regarding why DOI resolution has different effects on in-plane resolution and cross-plane resolution are being investigated.

(a) In-plane resolution, Row index =1

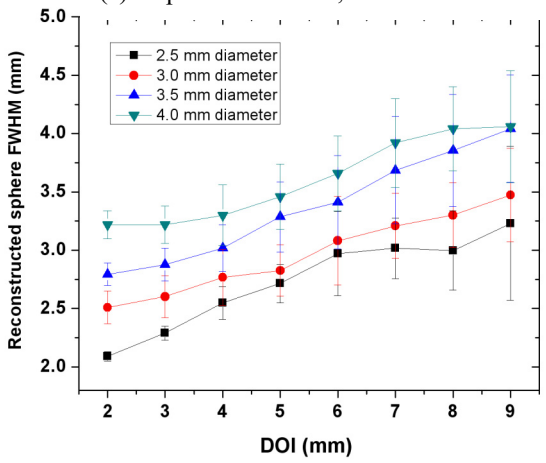


(b) Cross-plane resolution, Row index =1

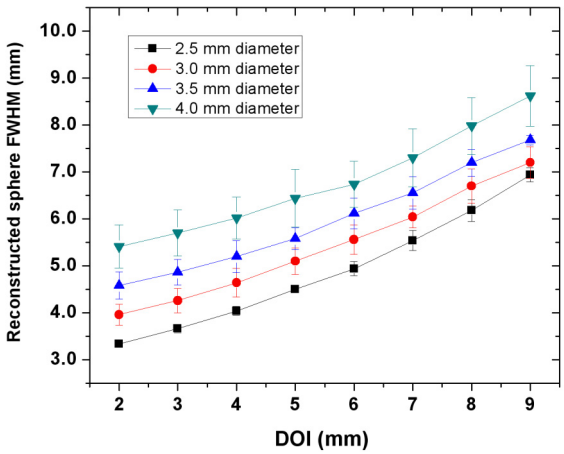


(c) In-plane resolution

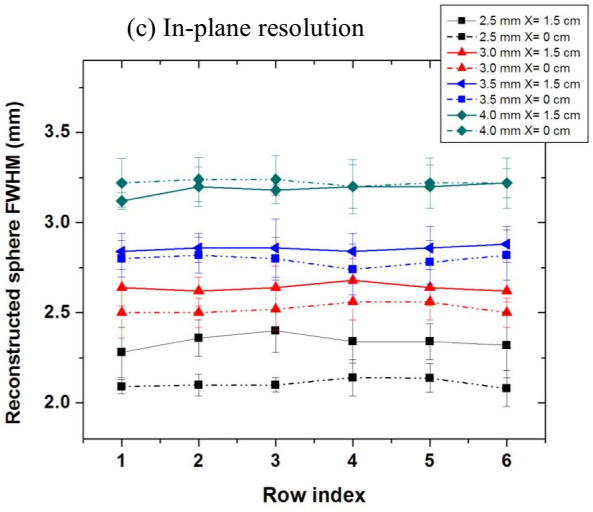


(d) Cross-plane resolution

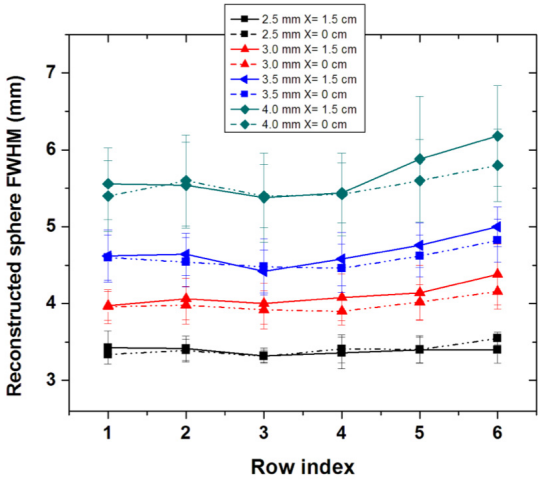


Fig. 6: The measured sphere FWHM as a function of DOI resolution for in-plane resolution (a) and cross-plane resolution (b) for X=0 and the panel separation is 4 cm. The resolution uniformity study for both central plane (X=0) and off-center plane (X=1.5 cm). The in-plane resolution is shown in (c) and the cross-plane resolution is shown in (d). DOI resolution is chosen to be 2 mm for the results in (c) and (d).

## V. CONCLUSIONS

This work studies the performance of a CZT dual PET dedicated for breast cancer. The improved geometry enables the system to achieve ~32% sensitivity for a point source at the center (4 cm panel separation). For a simplified breast phantom surrounded by heart and torso compartments, the peak NEC rate was studied to be ~42,000 cts/sec at the 10% energy window around 511 keV and 10 ns coincidence time window. The dependency of system in-plane and cross-plane resolution on DOI resolution (defined by cross-strip cathode pitch) was studied. The results can guide the design of cathode strip pitch to meet pre-defined reconstructed resolution and resolution uniformity requirements. We are working towards further optimizing the system by taking lesion contrast recovery into account and building a prototype CZT dual panel sub-system.

## IV. REFERENCES


[1] W. M. Moses, et al. "Instrumentation optimization for positron emission mammography", Nucl. Instr. Methods Phys Res. A, 527 76-82, 2004

[2] N. K. Doshi, et al. "Design and evaluation of an LSO PET detector for breast cancer imaging". Med Phys, 27 1535-43, 2000.

[3] R. R. Raylman, et al. "The potential role of positron emission mammography for detection of breast cancer: a phantom study", Med Phys, 27 1943-54, 2000.

[4] J. Zhang, et al. Study of the performance of a novel 1 mm resolution dual-panel PET camera design dedicated to breast cancer imaging using Monte Carlo Simulation. Med Phys, 34 1-14, 2007.

[5] C.S. Levin, et al. "Characteristics and Performance of Cadmium Zinc Telluride Detectors for Positron Emission Tomography", IEEE NSS/MIC, # M2-117, 2004.

[6] P. D. Olcott, et al. "GRAY: High Energy Photon Ray Tracer for PET applications", IEEE NSS/MIC, # M06-217, 2006.